NANO LETTERS

Letter

pubs.acs.org/NanoLett

Coherent Phonon Rabi Oscillations with a High-Frequency Carbon Nanotube Phonon Cavity

Dong Zhu,[†,‡] Xin-He Wang,[§,∥] Wei-Cheng Kong,[†,‡] Guang-Wei Deng,[†,‡] Jiang-Tao Wang,[§,∥] Hai-Ou Li,[†,‡] Gang Cao,[†,‡] Ming Xiao,[†,‡] Kai-Li Jiang,[§,∥] Xing-Can Dai,[§,∥] Guang-Can Guo,[†,‡] Franco Nori,[⊥,#] and Guo-Ping Guo*[,†,‡]

[†]Key Laboratory of Quantum Information, University of Science and Technology of China, Chinese Academy of Sciences, Hefei 230026, China

[‡]Synergetic Innovation Center of Quantum Information and Quantum Physics, University of Science and Technology of China, Hefei, Anhui 230026, China

[§]State Key Laboratory of Low-Dimensional Quantum Physics, Department of Physics and Tsinghua-Foxconn Nanotechnology Research Center, Tsinghua University, Beijing 100084, China

[∥]Collaborative Innovation Center of Quantum Matter, Beijing 100084, China

[⊥]CEMS, RIKEN, Wako-shi, Saitama 351-0198, Japan

[#]Physics Department, University of Michigan, Ann Arbor, Michigan 48109-1040, United States

Supporting Information

ABSTRACT: Phonon-cavity electromechanics allows the manipulation of mechanical oscillations similar to photon-cavity systems. Many advances on this subject have been achieved in various materials. In addition, the coherent phonon transfer (phonon Rabi oscillations) between the phonon cavity mode and another oscillation mode has attracted many interest in nanoscience. Here, we demonstrate coherent phonon transfer in a carbon nanotube phonon-cavity system with two mechanical modes exhibiting strong dynamical coupling. The gate-tunable phonon oscillation modes are manipulated and detected by extending the red-detuned pump idea of photonic cavity electromechanics. The first- and second-order coherent phonon transfers are observed with Rabi frequencies 591 and 125 kHz, respectively. The frequency quality factor product $fQ_m \sim 2 \times 10^{12}$ Hz achieved here is larger than $k_B T_{base}/h$, which may enable the future realization of Rabi oscillations in the quantum regime.

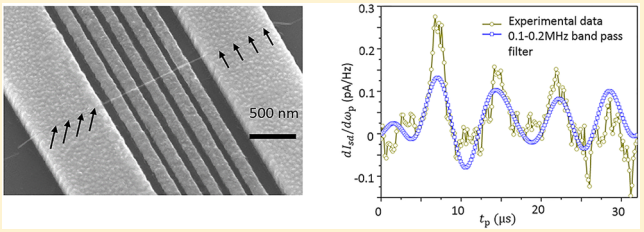

KEYWORDS: *Phonon cavity, nanotube, strong coupling, phonon rabi oscillations, quantum dot, electric tuning*

Mode coupling of mechanical resonators has recently attracted considerable attention in nanotechnology for both practical applications and fundamental studies, such as mass sensing,[1,2] charge detection,[3] band-pass filters,[4] signal amplification,[5] phonon-mediated electron interaction,[6] chaotic dynamics[7] and nonlinearity.[8−11]

To date, pioneering experiments have demonstrated classically coherent phonon manipulations in a single GaAs-based mechanical resonator[12] and two coupled GaAs-based mechanical beams[13] using dynamical coupling, and a SiN resonator[14] using a linear-coupling method different from the dynamical coupling used here. The manipulated phonon frequencies were of the order of 10 Hz, 100 kHz, and several MHz, respectively. The Rabi frequencies were typically around 40 Hz, 100 Hz, and 8 kHz, respectively. However, to further achieve coherent phonon manipulation in the quantum regime[15] ($fQ_m > k_B T_{base}/h$), higher-frequency mechanical resonators are also desirable due to fewer-phonon occupation at a fixed temperature T_{base}. For high-frequency resonators (such as carbon nanotubes,[16] MoS_2,[17] and graphene[18] systems), the large-frequency dispersion and the natural multimodes offer a platform to use the higher-frequency mode as a phononic cavity. Dynamical strong-mode couplings have been reported in previous works,[16−18] which show the advantage of coupling two mechanical modes with arbitrary frequency differences. Despite these remarkable achievements, there is still a lack of coherent phonon manipulation in these systems.[16−18]

Carbon nanotube (CNT) mechanical resonators[19−26] are well-known not only for their high-quality factors[24] and low mass but also for their high frequencies. Nonlinear strong mode-coupling in carbon nanotube resonators has been studied in a few works[9,10] while dynamical strong mode-coupling has not been implemented until very recently.[16] The exceptional properties of CNTs mean that the phonon Rabi oscillations

Received: October 8, 2016
Revised: December 15, 2016
Published: January 9, 2017

DOI: 10.1021/acs.nanolett.6b04223
Nano Lett. 2017, 17, 915−921

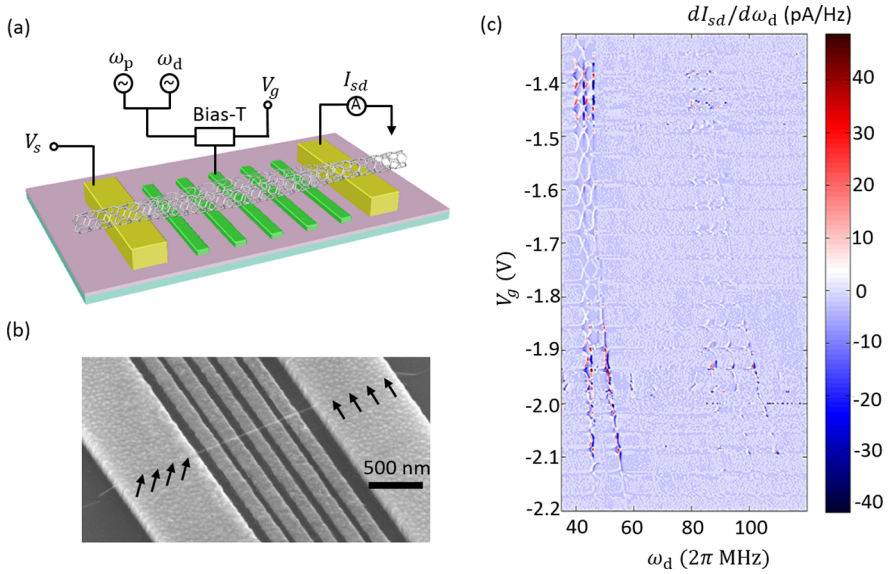

Figure 1. Carbon nanotube resonator with large frequency tunability of various flexural modes. (a) Schematic of the sample structure and the measurement circuit. A carbon nanotube (CNT) resonator is in contact with the source and drain electrodes (800 nm wide) and suspended over five gates (120 nm wide and spaced by 80 nm) with a trench of 1200 nm and a depth of 100 nm. (b) Scanning electron micrograph of the device with a scale bar of 500 nm. (c) Large-frequency tunability of various flexural modes with the middle gate voltage under a drive microwave power $P_d = -43$ dBm. Two distinct first mechanical modes (~50 MHz) and three second mechanical modes (~100 MHz) vary largely when changing the dc gate voltage. Here the derivative of the transport current with respect to the frequency of drive microwave $dI_{sd}/d\omega_d$ to remove the Coulomb blockade and clearly show all the possible mechanical modes (see the transport current data in Figure S2 of the Supporting Informations III).

implemented by a CNT phonon cavity should exhibit a superior performance.

In this Letter, we report the successful implementation of coherent phonon Rabi oscillations with an ~50 MHz resonant mechanical frequency in a CNT resonator. By combining previous ideas on the dynamical mode-coupling method in separate beams[17] and linear mode-coupling in a single resonator,[14] we achieved dynamical strong mode-coupling between two distinct modes in a single CNT resonator. Analogous to photonic cavity-mechanical systems,[27−31] the higher-frequency mode in our system can be treated as a phonon cavity[17,18,32] and the lower-frequency mode is shown to be parametrically coupled to this microwave phonon cavity. Coherent phonon transfers are observed in this mechanical phonon cavity system with Rabi frequency 591 kHz (for the first-order) and 125 kHz (for the second-order), respectively. Furthermore, the achieved frequency quality factor product, $fQ_m \sim 2 \times 10^{12}$ Hz, fulfills the standard to reach the quantum regime ($fQ_m > k_B T_{base}/h$) after further cooling.[15]

Results. We design and fabricate a carbon nanotube resonator suspended over the source and drain electrodes, which are 150 nm thick and 800 nm wide (Figure 1a). The trench is designed to be 1200 nm wide and 100 nm deep; also five gates (with 50 nm thickness and 120 nm width) are located underneath the CNT. The CNT is grown by chemical vapor deposition and is typically double-walled and about 2−3 nm in diameter. The inner shell tube of the double-walled CNT is then drawn out using a micromanipulation technique, which is then transferred and precisely positioned on the predesigned metal electrodes [source (S) and drain (D)]. The scanning electron microscope (SEM) picture (Figure 1b) shows that the CNT is suspended quite well over the gate electrodes and the sample is very clean.

The measurements are performed in a dry refrigerator Triton system with base temperature of approximately 10 mK and a pressure typically under 10^{-6} Torr. We use an electrical approach to actuate and detect the mechanical modes of the CNT. A biased voltage V_s is added to the S electrode and the direct current (dc) transport current I_{sd} of the CNT is measured at the D electrode with a commercial multimeter. We use a bias-Tee to apply both dc and alternating current (ac) voltages on the third of the five gates, where the dc voltage is used to tune the chemical potential of the quantum dot formed on the local region of the CNT above the gate and the ac voltage is used to actuate the CNT resonator. In this experiment, two pump and drive microwave signals (ω_p and ω_d) are combined on the ac port (Figure 1a). When the frequency of drive microwave ω_d approaches the resonance frequency of the CNT, the dc transport current I_{sd} shows a distinct peak as the signal of the mechanical vibration, which is due to the change of the displacement-modulated capacitance of the suspended CNT quantum dot (see Supporting Information I). The various vibrational modes are shown in Figure 1c with an input drive signal power $P_d = -43$ dBm, where two distinct mechanical modes of the first-order vibration (ω_1 for the lower frequency mode and ω_2 for the higher mode) with a frequency of approximately 50 MHz (varying largely when changing the dc gate voltage, approximately 20 MHz/V) are so strongly coupled to a quantum dot that they cannot be distinguished for small gate voltages. This phenomenon is due to the high drive power. We can reasonably infer that (1) the mode with lower resonant frequency mainly vibrates in-plane parallel to the gate electrode and (2) the higher mode vibrates out-of-the-plane because the electrostatic force between the gate and the CNT is stronger in the vertical direction so the vertical vibration tension in the CNT is larger than the parallel vibration tension, causing a larger spring effect.[10,33] Figure 1c also shows three weak mechanical modes of the second-order vibration with resonant frequencies of approximately 100 MHz. Because of the

DOI: 10.1021/acs.nanolett.6b04223
Nano Lett. 2017, 17, 915−921

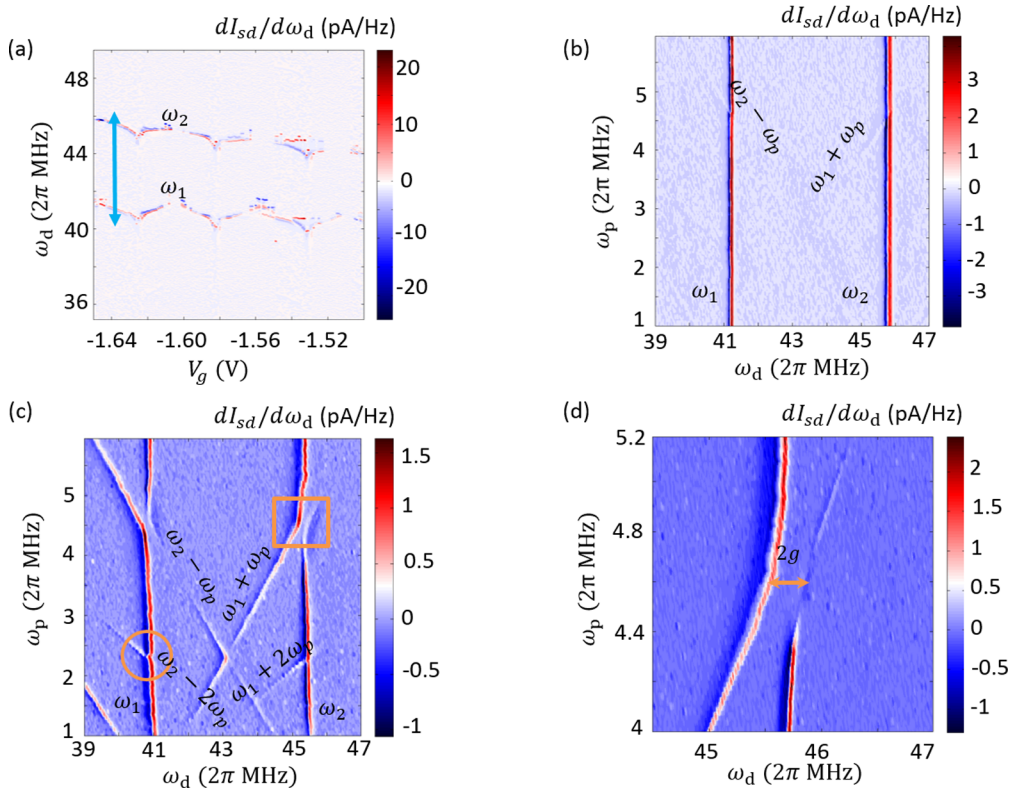

Figure 2. Dynamical strong mode-coupling via normal-mode splitting. (a) The two distinct first mechanical modes under a weak drive power of P_d = −70 dBm. The lower-frequency mode is denoted as "oscillation mode 1" and the higher-frequency mode is denoted as "phonon cavity mode 2". The normal-mode splitting is performed at the gate voltage V_g = −1.64 V (see the arrow). (b) The Stokes and anti-Stokes sidebands of the two modes with a pump power P_p = −49 dBm. Only the first-order sidebands are shown because of the weak pump power. These sidebands cause dynamical coupling between the oscillation mode and phonon cavity mode. (c) First-order normal-mode splitting with a higher pump power P_p = −44 dBm, when the pump frequency ω_p approaches $\Delta\omega$ (see the rectangle). Both the oscillation mode and the phonon cavity mode show strong dynamical mode-coupling. The second-order mode-coupling is not apparent at $\omega_p = \Delta\omega/2$ for the low-pump power (see the circle). Both first- and second-order Stokes and anti-Stokes sidebands of the two mode are shown. (d) Larger normal mode splitting of the phonon cavity at $\omega_p = \Delta\omega$ with a pump power P_p = −34 dBm. The coupling rate is approximately $g = 2\pi \times 225$ kHz (see the arrow).

symmetric structure of our measurement scheme, the vibration modes with an odd number of wave nodes cannot apparently change the capacity between the gate and the CNT. The resonant frequencies for the first vibration modes (∼50 MHz) and second vibration modes (∼100 MHz) are approximately in agreement with the elastic string model,[33] which has a simple relation on the multiple higher-vibration frequencies and first-vibration frequencies, $f_n = nf_1$.

In this experiment, the two distinct mechanical modes of the first-order vibration are selected to implement the phonon Rabi oscillations or coherent phonon manipulations. Hereafter, we denote the lower-frequency mode as oscillation mode 1 and the higher-frequency mode as phonon cavity mode 2. To improve the quality factor of the resonator, the drive microwave power is further reduced to P_d = −70 dBm, and Figure 2a shows the resonant frequencies of modes 1 and 2 with different dc gate voltages measured by single-electron tunneling. Under weak-drive microwave power, modes 1 and 2 are distinctly separated from each other, with a frequency difference $\Delta\omega \sim 2\pi \times 5$ MHz. The quality factors for both modes are ∼50 000, and the corresponding decoherence rate $\gamma \sim 2\pi \times 900$ Hz.

We further perform a strong dynamical coupling between oscillation mode 1 and the phonon cavity mode 2 by showing the normal-mode splitting for which a red-detuned (relative to the phonon cavity mode) parametric pump microwave ω_p ($\omega_p \approx \omega_2 - \omega_1 = \Delta\omega$) is applied to the CNT combined with the previous drive microwave ω_d with P_d = −70 dBm (see Figure 1a). By applying a gate voltage V_g = −1.64 V, we tune the oscillation mode 1 frequency to $\omega_1 = 2\pi \times 41.12$ MHz and the resonant frequency of the phonon cavity mode to $\omega_2 = 2\pi \times 45.68$ MHz and $\Delta\omega = 2\pi \times 4.56$ MHz, which are shown by the arrow in Figure 2a. Figure 2b shows the two modes while scanning the pump microwave frequency with a pump power P_p = −49 dBm. The Stokes and anti-Stokes sidebands of the two modes emerge and these sidebands cause dynamical coupling between the oscillation mode and phonon cavity mode. $dI_{sd}/d\omega_d$ is used in Figure 2b–d to reduce the noise and clearly show the coupling between the two mechanical modes. Here at different pump frequency ω_p, we measure the transport current as scanning the drive frequency ω_d and the noise is produced along the axis of pump frequency ω_p. Normal-mode splitting is demonstrated in Figure 2c for both modes with a slightly larger pump power P_p = −44 dBm, when the pump frequency ω_p approaches $\Delta\omega$. The pumped microwaves produce a series of sidebands of the two modes with phonon frequency $\omega_{1,2} \pm n\omega_p$. When the Stokes sideband of mode 2 matches the resonance frequency of mode 1, that is, $\hbar\omega_1 \sim (\hbar\omega_2 - \hbar\omega_p)$, or the anti-Stokes sideband of mode 1 matches the resonance frequency of mode 2, $\hbar\omega_2 \sim (\hbar\omega_1 + \hbar\omega_p)$, avoided crossing occurs. This avoided crossing signifies that dynamical coupling between the oscillation mode and the phonon cavity is in the strong-coupling regime. The coupling

DOI: 10.1021/acs.nanolett.6b04223
Nano Lett. 2017, 17, 915–921

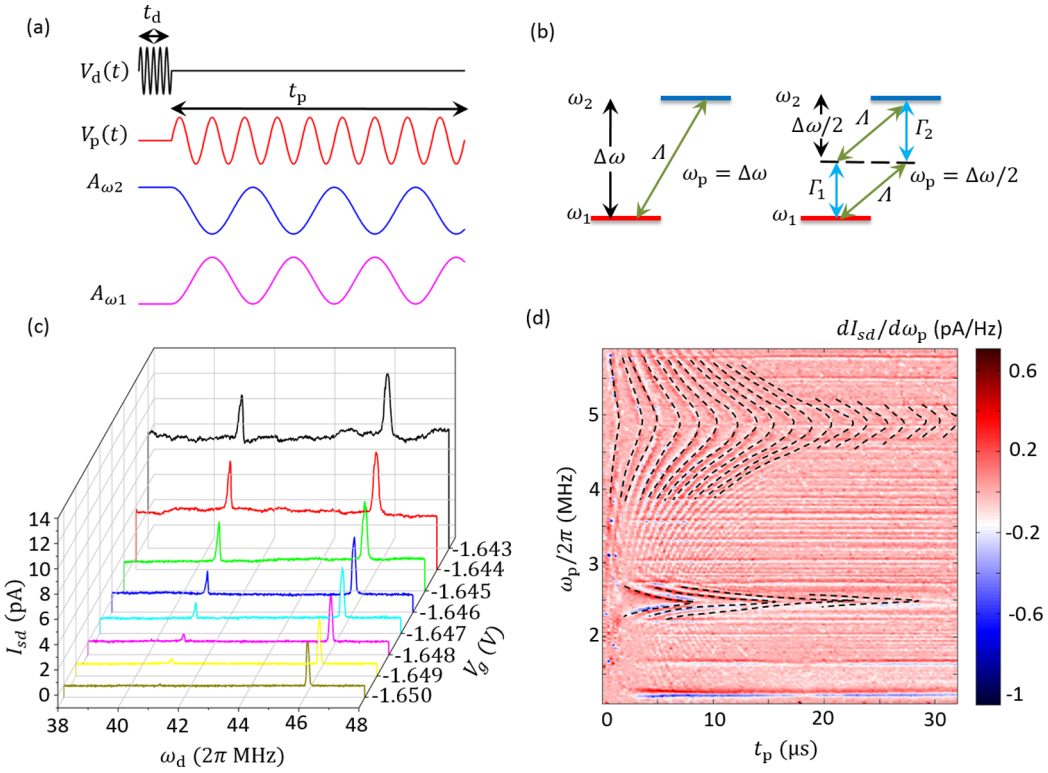

Figure 3. Phonon Rabi oscillation between the oscillation mode and phonon cavity mode. (a) The time-domain pulse sequence used to implement phonon Rabi oscillations. (b) Schematic of first- and second-order phonon Rabi oscillation processes. (c) dc transport current by scanning the drive microwave frequency with different gate voltages from −1.643 to −1.650 V. The voltage step is −0.001 V and drive power P_p = −53 dBm. (d) Phonon Rabi oscillations with a large pump power P_p = −3 dBm. Nineteen distinct cycles of coherent energy exchanges between the oscillation mode and the phonon cavity mode at $\omega_p = \Delta\omega = 2\pi \times 4.9$ MHz (the first order) are shown and 4 cycles of second-order coherent energy exchange at $\omega_p = \Delta\omega/2 = 2\pi \times 2.45$ MHz are also observed for the large pump power. $dI_{sd}/d\omega_p$ is used again to increase the signal-to-noise ratio. Here at different pump time t_p, we measure the transport current as scanning the pump frequency ω_p and the noise is produced along the axis of pump time t_p. The original results is provided in Figure S5 in Supporting Information VI.

strength g is about half the frequency splitting (Figure 2d) and can also be tuned by the amplitude of the pump microwave. Figure 2d shows the normal-mode splitting of the phonon cavity mode ω_2 with a larger pump power P_p = −34 dBm, and the coupling rate is increased to be $g = 2\pi \times 225$ kHz. This is much larger than that in GaAs-based mechanical resonators[13,32] (typically 100 Hz) and approximately 27 times larger than in silicon nitride devices[14] (8.3 kHz) that use a linear coupling method different to the dynamical coupling used here. The strong coupling between the oscillation mode and the phonon cavity can also be quantified by a figure of merit called cooperativity, defined as $C = 4g^2/(\gamma_1\gamma_2)$, which is ∼250 000 in our system and much higher than that in graphene[18] (C as high as 60), MoS_2 resonators[17] (C = 2066), and GaAs-based mechanical resonators[13] (C = 90). The frequency quality factor product $fQ_m \sim 2 \times 10^{12}$ Hz in our device is also the highest compared with that reported in other similar studies,[13,17,18,32] and is very close to the standard of phonon-cavity mechanics in the quantum regime[15] at room temperature ($fQ_m > k_B T_{room}/h$).

The strong dynamical coupling between the oscillation mode ω_1 and the phonon cavity mode ω_2 offers a platform for coherent phonon transfer between a phonon cavity and an oscillator (phonon Rabi oscillation). Figure 3a shows the time-domain pulse sequence we used to achieve this goal. The detailed measurement scheme of the phonon Rabi oscillation is discussed in Supporting Information V. First, a drive microwave with frequency ω_d, matching the phonon cavity resonant frequency ω_2, is applied to actuate the phonon cavity mode for ∼t_d and then turned off, which is realized by a frequency mixer and arbitrary waveform generator (AWG). At the time when the drive microwave is turned off, the red-detuned parametric pump microwave with $\omega_p = \omega_2 - \omega_1 = \Delta\omega$ is turned on for a time t_p, which causes the coherent energy exchange between the phonon cavity and the oscillation mode. This is the first-order coherent process (n = 1). The second-order coherent process (n = 2) occurs for the case when $\omega_p = \Delta\omega/2$, while the normal-mode splitting for this case is not apparent in Figure 2c (the circle).

For the single CNT resonator, we have to identify the contributions from each of the two modes to the dc transport current to manipulate the phonon Rabi oscillation. However, this is very difficult when both of the two modes exist at the same time, because the influence of mechanical vibrations on the transport current through single-electron tunneling is an average effect for high-frequency motion. To solve this problem, we introduce a useful and novel refinement in our experiment. By carefully changing the gate voltage, we find that the oscillation mode 1 can be tuned to where the transport current is not sensitive, so that only the phonon cavity mode 2 can be detected, which is further used to perform the phonon Rabi oscillations (See Supporting Information VII). Figure 3c shows the dc transport current when scanning the drive microwave frequency for different gate voltages from −1.643 to −1.650 V in steps of −0.001 V. Note that when the gate voltage is smaller than −1.646 V, the oscillation mode with lower resonant frequency cannot be sensitively detected by the dc

DOI: 10.1021/acs.nanolett.6b04223
Nano Lett. 2017, 17, 915−921

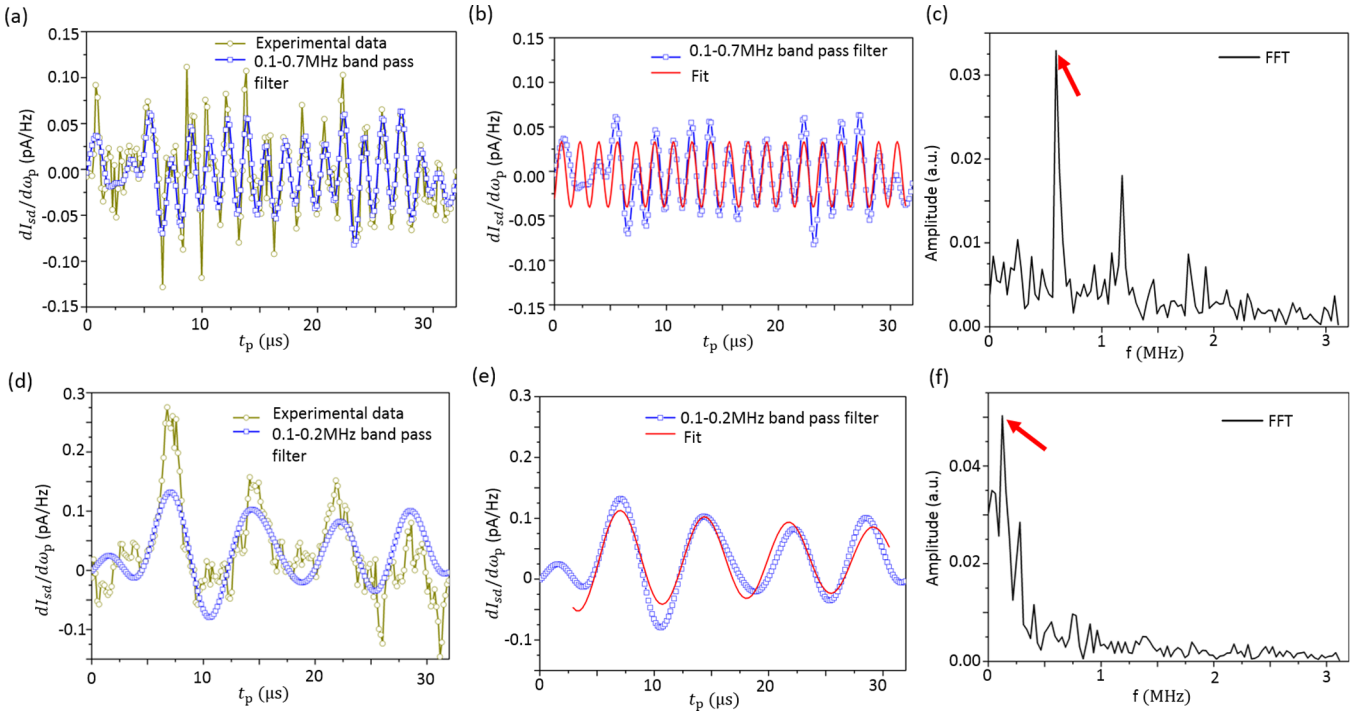

Figure 4. Fitting the time domain data for the phonon Rabi coupling rate. (a) First-order phonon Rabi oscillations at $\omega_p = \Delta\omega = 2\pi \times 4.9$ MHz from Figure 3d. Data in dark yellow are the experimental data and the data in blue are under a 0.1−0.7 MHz band-pass filter of the experimental data, which are in good agreement with the guide lines shown in Figure 3d. (b) The first-order coupling rate is as high as $g_1 = 2\pi \times 591$ kHz by fitting the filtered data. (c) The FFT of the experimental data shows a distinct peak at 591 kHz (see the arrow). (d) Second-order phonon Rabi oscillations at $\omega_p = \Delta\omega/2 = 2\pi \times 2.45$ MHz from Figure 3(d). Data in dark yellow are the experimental data and the data in blue are under a 0.1−0.2 MHz band-pass filter of the experimental data, which is in good agreement with the guide lines in Figure 3d. (e) Second-order coupling rate is $g_2 = 2\pi \times 125$ kHz by fitting the filtered data. (f) The FFT of the experimental data shows a distinct peak at 125 kHz (see the arrow).

transport current, while the phonon cavity mode with a higher resonant frequency is not affected. When gate voltage is −1.649 or −1.650 V, the oscillation mode is almost entirely not detected by the current, which enables us to only detect the phonon cavity mode when there is an energy exchange between these two modes caused by the pump. By applying a gate voltage $V_g = -1.650$ V, we tune the oscillation mode 1 frequency to $\omega_1 = 2\pi \times 41.20$ MHz and the resonant frequency of the phonon cavity mode to $\omega_2 = 2\pi \times 46.10$ MHz and $\Delta\omega = 2\pi \times 4.9$ MHz. Figure 3d shows the phonon Rabi oscillations with pump power $P_p = 3$ dBm. The drive power is $P_p = -53$ dBm and the drive frequency matches the phonon cavity mode $\omega_2 = 2\pi \times 46.10$ MHz. The higher drive power allows the phonon cavity mode with a larger amplitude that will help to increase the electric signal strength of the Rabi oscillations, while the quality factor will decrease because of the stronger coupling between single-electron tunneling and nanomechanical motion.[21] The dc transport current dependence at $\omega_p = \Delta\omega = 2\pi \times 4.9$ MHz shows 19 distinct cycles of energy exchanges between the oscillation mode and the phonon cavity mode that is better than the results (8 cycles) obtained from two coupled GaAs-based mechanical resonators.[13] The second-order process at $\omega_p = \Delta\omega/2 = 2\pi \times 2.45$ MHz with 4 cycles of energy exchanges is shown in Figure 3d, and is a bit weaker than the first-order ones.

To understand the dynamics of the phonon Rabi oscillation, we model the dynamics of our system using two coupled vibration modes with a time-varying spring constant. The Hamiltonian[32] is

$$H = \frac{p_c^2}{2m_{eff}} + \frac{1}{2}m_{eff}(\omega_2^2 + \Gamma_2 V_p^2 \cos(\omega_p t))q_c^2 + \frac{p_o^2}{2m_{eff}} + \frac{1}{2}m_{eff}(\omega_1^2 + \Gamma_1 V_p^2 \cos(\omega_p t))q_o^2 + m_{eff}\Lambda V_p^2 \cos(\omega_p t) q_c q_o$$

where q_o, p_o represent the oscillation mode 1 and q_c, p_c represent the phonon cavity mode 2. Also, Λ is the intermodal coupling coefficient and $\Gamma_{1,2}$ are the intramodal coupling coefficients for mode 1 and mode 2, respectively. The effective mass of the two modes are not distinguished as discussed in Supporting Information II. Figure 3b shows the schematics of the first- and second-order phonon Rabi oscillation processes. For the first-order coherent process, the intermodal coupling term ΛV_p^2 is responsible for the energy exchange, with the pump frequency matching the frequency difference of the two modes $\omega_p = \Delta\omega$. Additionally, the coupling rate[13,17,18] is given by $g \sim \frac{\Lambda V_p^2}{2\sqrt{\omega_1\omega_2}}$. For the second coherent process, the intermodal coupling term ΛV_p^2 combined with the intramodal coupling term $\Gamma_{1,2}V_p^2$ is responsible for the higher-order energy exchange between the modes (Figure 3b).

The coupling rate, or the Rabi frequency, g can be determined by fitting the time-domain data of the energy-exchange rate at $\omega_p = \Delta\omega$ and $\omega_p = \Delta\omega/2$, respectively. Figure 4a,d shows the first-order and second-order coherent phonon Rabi oscillations, respectively, between the oscillation mode 1 and the phonon cavity mode 2. For the first-order oscillation, a 0.1−0.7 MHz band-pass filter is used to remove the noise signal of the experimental data. As a result, the filtered signal in Figure 4a is in good agreement with the guide lines in Figure 3d. The first-order coupling rate is $g_1 = 2\pi \times 591$ kHz by fitting the

DOI: 10.1021/acs.nanolett.6b04223
Nano Lett. 2017, 17, 915−921

filtered data (Figure 4b), which agrees with the fast Fourier transform (FFT) of the original experimental data (see the arrow in Figure 4c). Similarly, the second-order coupling rate is $g_2 = 2\pi \times 125$ kHz by fitting the filtered data with a 0.1 MHz−0.2 MHz band-pass filter (Figure 4e), which also agrees with the FFT of the original experimental data (see the arrow in Figure 4f). The coupling rate is higher than the previous normal-mode splitting experiment (Figure 2c) because of the large pump power used here. Compared again with similar studies for GaAs-based mechanical resonators[13] and silicon nitride devices,[14] our result is ∼5900 times larger than that for GaAs-based mechanical resonators (typically ∼100 Hz) and about 70 times larger than that for silicon nitride devices (8.3 kHz).

Conclusion. We have demonstrated coherent phonon transfer between two mechanical modes of a carbon nanotube resonator. Similar to photonic cavity electro-mechanics,[27−32] the red-detuned pump technique is used to demonstrate the normal-mode splitting of the oscillation mode (low-frequency mode) and the phonon cavity (high-frequency mode). An electromagnetic pulse[13,14] is applied to implement the coherent phonon Rabi oscillations in this phonon-cavity mechanical system. Compared with previous studies,[12−14,17,18,32] the present study shows higher-frequency classical phonon Rabi oscillations, a larger cooperativity C, and a higher-frequency quality-factor product[15] ($fQ_m > k_B T_{base}/h$). The methods demonstrated here can be applied to other mechanical systems such as MoS_2 or graphene resonators[17,18] and will also be highly valuable for future studies of quantum phonon cavity systems and electron−phonon coupling[20,21,23,34]

■ ASSOCIATED CONTENT

Supporting Information

The Supporting Information is available free of charge on the ACS Publications website at DOI: 10.1021/acs.nanolett.6b04223.

Additional information, figures, and references (PDF)

■ AUTHOR INFORMATION

Corresponding Author

*E-mail: gpguo@ustc.edu.cn.

ORCID

Guo-Ping Guo: 0000-0002-2179-9507

Author Contributions

D.Z., X.-H.W., and W.-C.K. contributed equally to this work.

Notes

The authors declare no competing financial interest.

■ ACKNOWLEDGMENTS

This work was supported by the National Key R&D Program (Grant 2016YFA0301700), the Strategic Priority Research Program of the CAS (Grant XDB01030000), the National Natural Science Foundation (Grants 11304301, 11575172, 61306150, and 91421303), and the Fundamental Research Fund for the Central Universities. It was also partially supported by a Grant-in-Aid for Scientific Research (A), and a grant from the John Templeton Foundation.

■ REFERENCES

(1) Spletzer, M.; Raman, A.; Wu, A. Q.; Xu, X. F.; Reifenberger, R. *Appl. Phys. Lett.* **2006**, *88* (25), 254102.

(2) Gil-Santos, E.; Ramos, D.; Jana, A.; Calleja, M.; Raman, A.; Tamayo, J. *Nano Lett.* **2009**, *9* (12), 4122−7.

(3) Okamoto, H.; Kitajima, N.; Onomitsu, K.; Kometani, R.; Warisawa, S.; Ishihara, S.; Yamaguchi, H. *Appl. Phys. Lett.* **2011**, *98* (1), 014103.

(4) Bannon, F. D.; Clark, J. R.; Nguyen, C. T.-C. *IEEE J. Solid-State Circuits* **2000**, *35* (4), 512.

(5) Karabalin, R. B.; Lifshitz, R.; Cross, M. C.; Matheny, M. H.; Masmanidis, S. C.; Roukes, M. L. *Phys. Rev. Lett.* **2011**, *106* (9), 094102.

(6) Deng, G. W.; Zhu, D.; Wang, X. H.; Zou, C. L.; Wang, J. T.; Li, H. O.; Cao, G.; Liu, D.; Li, Y.; Xiao, M.; Guo, G. C.; Jiang, K. L.; Dai, X. C.; Guo, G. P. *Nano Lett.* **2016**, *16* (9), 5456−62.

(7) Karabalin, R. B.; Cross, M. C.; Roukes, M. L. *Phys. Rev. B: Condens. Matter Mater. Phys.* **2009**, *79*, 16.

(8) Westra, H. J.; Poot, M.; van der Zant, H. S.; Venstra, W. J. *Phys. Rev. Lett.* **2010**, *105* (11), 117205.

(9) Castellanos-Gomez, A.; Meerwaldt, H. B.; Venstra, W. J.; van der Zant, H. S. J.; Steele, G. A. *Phys. Rev. B: Condens. Matter Mater. Phys.* **2012**, *86*, 041402.

(10) Eichler, A.; del Alamo Ruiz, M.; Plaza, J. A.; Bachtold, A. *Phys. Rev. Lett.* **2012**, *109* (2), 025503.

(11) Eriksson, A. M.; Midtvedt, D.; Croy, A.; Isacsson, A. *Nanotechnology* **2013**, *24* (39), 395702.

(12) Mahboob, I.; Nier, V.; Nishiguchi, K.; Fujiwara, A.; Yamaguchi, H. *Appl. Phys. Lett.* **2013**, *103* (15), 153105.

(13) Okamoto, H.; Gourgout, A.; Chang, C.-Y.; Onomitsu, K.; Mahboob, I.; Chang, E. Y.; Yamaguchi, H. *Nat. Phys.* **2013**, *9* (8), 480−484.

(14) Faust, T.; Rieger, J.; Seitner, M. J.; Kotthaus, J. P.; Weig, E. M. *Nat. Phys.* **2013**, *9* (8), 485−488.

(15) Norte, R. A.; Moura, J. P.; Groblacher, S. *Phys. Rev. Lett.* **2016**, *116* (14), 147202.

(16) Li, S. X.; Zhu, D.; Wang, X. H.; Wang, J. T.; Deng, G. W.; Li, H. O.; Cao, G.; Xiao, M.; Guo, G. C.; Jiang, K. L.; Dai, X. C.; Guo, G. P. *Nanoscale* **2016**, *8* (31), 14809−13.

(17) Liu, C. H.; Kim, I. S.; Lauhon, L. J. *Nano Lett.* **2015**, *15* (10), 6727−31.

(18) Mathew, J. P.; Patel, R. N.; Borah, A.; Vijay, R.; Deshmukh, M. M. *Nat. Nanotechnol.* **2016**, *11* (9), 747−51.

(19) Sazonova, V.; Yaish, Y.; Ustunel, H.; Roundy, D.; Arias, T. A.; McEuen, P. L. *Nature* **2004**, *431* (7006), 284−7.

(20) Lassagne, B.; Tarakanov, Y.; Kinaret, J.; Garcia-Sanchez, D.; Bachtold, A. *Science* **2009**, *325* (5944), 1107−10.

(21) Steele, G. A.; Huttel, A. K.; Witkamp, B.; Poot, M.; Meerwaldt, H. B.; Kouwenhoven, L. P.; van der Zant, H. S. *Science* **2009**, *325* (5944), 1103−7.

(22) Eichler, A.; Moser, J.; Chaste, J.; Zdrojek, M.; Wilson-Rae, I.; Bachtold, A. *Nat. Nanotechnol.* **2011**, *6* (6), 339−42.

(23) Benyamini, A.; Hamo, A.; Kusminskiy, S. V.; von Oppen, F.; Ilani, S. *Nat. Phys.* **2014**, *10* (2), 151−156.

(24) Moser, J.; Eichler, A.; Guttinger, J.; Dykman, M. I.; Bachtold, A. *Nat. Nanotechnol.* **2014**, *9* (12), 1007−11.

(25) Moser, J.; Guttinger, J.; Eichler, A.; Esplandiu, M. J.; Liu, D. E.; Dykman, M. I.; Bachtold, A. *Nat. Nanotechnol.* **2013**, *8* (7), 493−6.

(26) Schneider, B. H.; Singh, V.; Venstra, W. J.; Meerwaldt, H. B.; Steele, G. A. *Nat. Commun.* **2014**, *5*, 5819.

(27) Teufel, J. D.; Donner, T.; Li, D.; Harlow, J. W.; Allman, M. S.; Cicak, K.; Sirois, A. J.; Whittaker, J. D.; Lehnert, K. W.; Simmonds, R. W. *Nature* **2011**, *475* (7356), 359−63.

(28) Teufel, J. D.; Li, D.; Allman, M. S.; Cicak, K.; Sirois, A. J.; Whittaker, J. D.; Simmonds, R. W. *Nature* **2011**, *471* (7337), 204−8.

(29) Palomaki, T. A.; Harlow, J. W.; Teufel, J. D.; Simmonds, R. W.; Lehnert, K. W. *Nature* **2013**, *495* (7440), 210−4.

(30) Singh, V.; Bosman, S. J.; Schneider, B. H.; Blanter, Y. M.; Castellanos-Gomez, A.; Steele, G. A. *Nat. Nanotechnol.* **2014**, *9* (10), 820−4.

(31) Weber, P.; Guttinger, J.; Tsioutsios, I.; Chang, D. E.; Bachtold, A. *Nano Lett.* **2014**, *14* (5), 2854−60.

DOI: 10.1021/acs.nanolett.6b04223
Nano Lett. 2017, 17, 915−921

(32) Mahboob, I.; Nishiguchi, K.; Okamoto, H.; Yamaguchi, H. *Nat. Phys.* **2012**, *8* (5), 387−392.
(33) Ustunel, H.; Roundy, D.; Arias, T. A. *Nano Lett.* **2005**, *5* (3), 523−6.
(34) Li, P. B.; Xiang, Z. L.; Rabl, P.; Nori, F. *Phys. Rev. Lett.* **2016**, *117* (1), 015502.

DOI: 10.1021/acs.nanolett.6b04223
Nano Lett. 2017, 17, 915−921